

## Article

# sEMG-Upper Limb Interaction Force Estimation Framework Based on Residual Network and Bidirectional Long Short-Term Memory Network

Wei Lu <sup>1,2</sup> , Lifu Gao <sup>1,2</sup>, Huibin Cao <sup>1,2,\*</sup> and Zebin Li <sup>1,2,3,\*</sup> 

<sup>1</sup> Institute of Intelligent Machines, Hefei Institutes of Physical Science, Chinese Academy of Sciences, Hefei 230031, China

<sup>2</sup> Department of Science Island, University of Science and Technology of China, Hefei 230026, China

<sup>3</sup> School of Electrical and Photoelectric Engineering, West Anhui University, Lu'an 237012, China

\* Correspondence: hbcao@iim.ac.cn (H.C.); zebinli@163.com (Z.L.)

**Abstract:** It is of great significance to estimate the interaction force of upper limbs accurately for improving the control performance of human–computer interaction. However, due to the randomness of the input biological signals and the influence of environmental interference, the interaction force is difficult to estimate using the current methods. Therefore, based on the advantages of the Residual Network (ResNet) and Bidirectional Long Short-Term Memory Network (BiLSTM) model, this paper proposes an end-to-end regression model that integrates ResNet and BiLSTM with an attention mechanism. This model is more suitable for time series sEMG signals. Moreover, it improves the feature extraction ability of the signal and improves the accuracy of interaction force estimation. Experimental results show that this method can automatically extract effective features without professional knowledge. In addition, our method is superior to existing methods in estimation accuracy and generalization ability.

**Keywords:** electromyography; residual network; bidirectional long short-term memory network; interaction force estimation



**Citation:** Lu, W.; Gao, L.; Cao, H.; Li, Z. sEMG-Upper Limb Interaction Force Estimation Framework Based on Residual Network and Bidirectional Long Short-Term Memory Network. *Appl. Sci.* **2022**, *12*, 8652. <https://doi.org/10.3390/app12178652>

Academic Editor: Yu-Dong Zhang

Received: 9 July 2022

Accepted: 25 August 2022

Published: 29 August 2022

**Publisher's Note:** MDPI stays neutral with regard to jurisdictional claims in published maps and institutional affiliations.



**Copyright:** © 2022 by the authors. Licensee MDPI, Basel, Switzerland. This article is an open access article distributed under the terms and conditions of the Creative Commons Attribution (CC BY) license (<https://creativecommons.org/licenses/by/4.0/>).

## 1. Introduction

With the global increase in the older population and the demand for assisted rehabilitation for hemiplegia patients, various exoskeleton rehabilitation assistance robots are being developed. To improve the control performance of the assistance robots, the biggest challenge is to rapidly and accurately recognize the intention of human action [1]. At present, there are mainly the following ways to realize motion intention recognition [2,3]: mechanomyography (MMG), Surface electromyography (sEMG), electroencephalography (EEG), and electrocardiography (ECG).

The surface electromyography (sEMG) signal is a biological electrical signal produced by human muscle contraction. It has been extensively used to obtain human motion intention in wearable robot systems because of its effectiveness, portability, non-trauma, and non-delay features [4–7]. Different motion modes produce different frequencies and amplitudes of sEMG signals. Therefore, a wealth of information can be drawn from sEMG signals. Researchers have shown that the estimation of joint interaction force based on sEMG is one of the most effective ways to realize motion intention recognition [8]. There are two widely used methods to define the relationship between the sEMG signal and force: parametric-based and nonparametric-based. Muye et al. [9] used the Hill-type musculoskeletal model to design a quantitative method for the representation of the elbow joint force estimation. Romero et al. [10] proposed an interaction force estimate method by using the tendon length and contraction velocity obtained from sEMG and inverse dynamics analysis. Buchanan et al. [11] presented a forward dynamic neuromusculoskeletal

model which can be used to estimate and predict joint moments and muscle forces. Mitsuhiro et al. [12] presented a model which allows the estimation of muscle force from EMG signals associated with a physiology-based model of underlying microtubule dynamics. Youngjin Na et al. [13] proposed a force estimation method by combining a biomechanical muscle model with sEMG signal peaks. Na et al. [14] proposed a muscle-twitch model to estimate the muscle force in fatigue conditions. Nevertheless, since all these methods need to know the exact parameters of the muscle model, the convergence of the parameters is sensitive to computational time and complexity. A nonparametric algorithm is proposed to find the relationship between the sEMG signal and force.

As for nonparametric-based methods, machine learning-powered force estimation methods have become an effective tool in muscle force estimation and action recognition. A large variety of deep learning methods have been used in the biomedical field [15–23]. For instance, Youn et al. [15] systematically studied the feasibility of MMG for estimating the elbow interaction force at the wrist under an isometric contraction by using an artificial neural network in comparison with sEMG. In [16], an SVR model is proposed to estimate knee joint muscle force based on the MMG signal. Allouch S et al. [17] combined PCA and a Laplacian arrangement to fit the relationship between sEMG and muscle force. Xia et al. [18] proposed a model based on deep learning to estimate kinematic information from multi-channel sEMG signals. Duan et al. [19] presented a novel method based on multi-sensors to realize six gesture recognition tasks. DWT was used to realize the time-domain feature extraction of signals, and WNN was used to realize the action classification task. Experimental results show that the action classification accuracy of the proposed method is 94.67%, and is superior to the traditional ANN network. Wu et al. [20] proposed a CNN–SVM combined model to make use of their advantages for pattern recognition of knee motion. Xie et al. [21] applied a Long Short–Term–Memory (LSTM) neural network model for estimating the acceleration of the knee joint. Luo et al. [22] proposed a three domains fuzzy wavelet neural network (TDFWNN) algorithm without prior knowledge of the biomechanical model to estimate force through sEMG. In [23], Aviles et al. presented a method for estimating the applied forces that are based on using fuzzy theory and deep learning. However, parameter optimization is a difficult and important task for machine learning methods. Furthermore, the crucial problem is that the gradient of the error function vanishes easily after back–propagation.

It can be concluded from the above analysis that the means of obtaining timely and accurate interaction force estimation in advance is an enormous challenge. This study is aimed at resolving this challenging problem. That is to say, it proposes a timely and accurate estimation of human interaction force for a musculature–driven human–machine system. A novel deep learning framework is presented to accurately estimate the elbow interaction force. We selected ResNet, which is the latest CNN to automatically extract the valid feature of sEMG, instead of the manual way because it provides outstanding performance in terms of feature extraction. Subsequently, the BiLSTM network with attention mechanism was selected to map the nonlinear relationship between sEMG features and interaction force. To verify the estimation results, the experimental condition was selected as the elbow flexion in the horizontal plane during isometric contraction. The outline of our approach is illustrated in Figure 1. The purpose of this study is to demonstrate the feasibility of estimating elbow interaction force during isometric contraction based on a deep learning algorithm. To highlight the advantages of muscle force estimation which we proposed, we compared our algorithm with other mainstream force estimation algorithms in the experiment. The main contributions are summarized as follows:

1. Our framework can automatically extract the features of the sEMG signal and capture the local dependence between the data.
2. By introducing the attention mechanism, we can capture the salient structures of input data and explore the correlations among multiple dimensions of data, improving the learning performance of the model.

3. Our framework overall outperforms the non-ensemble methods in accuracy. In addition, the training time and testing time of the network are the shortest among other reported methods.

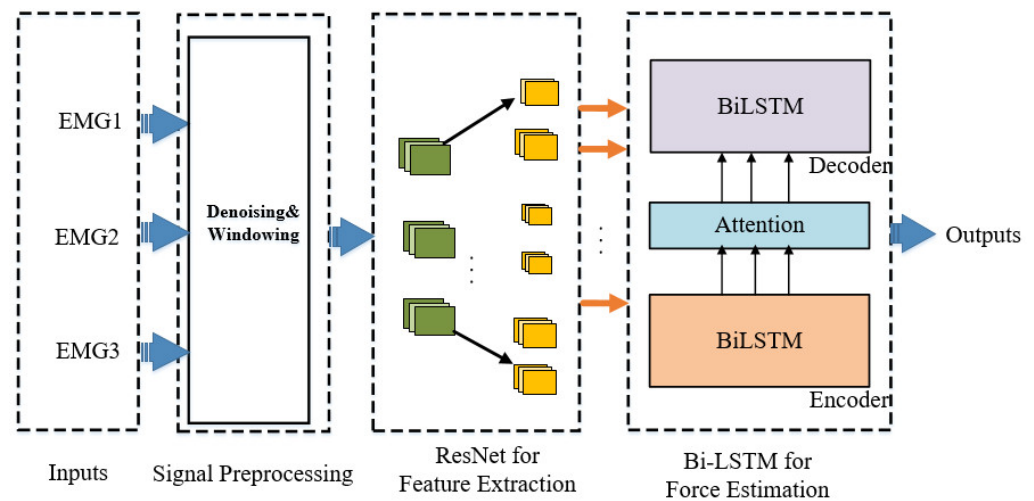


**Figure 1.** The framework of our method.

## 2. Materials and Methods

### 2.1. Elbow Anatomy Model Analysis

Isometric contraction refers to muscle contractions in which the length of a muscle remains constant and the tension changes. During this contractility, muscle tension can be maximized. Studies show that [24], when muscles contract at non-isometric speed, muscle force is not only related to sEMG signal strength but also to joint motion angle, muscle shape, muscle fatigue degree, and other factors. Therefore, when under isometric contraction conditions, muscle length remains constant, and only tension changes. Elbow interaction force was positively correlated with the amplitude of the sEMG signal. Therefore, acquired sEMG signals may have specific significance for reflecting the activity state of elbow interaction force. In this study, we intend to adopt the different angles of the elbow joint during isometric contraction to analyze the relationship between elbow interaction force and sEMG signals.

Figure 2 depicts the major contribution of the muscle under the isometric contraction of the elbow joint [25]. Therefore, we can consider that the major muscles involved in the completion of isometric contractions are the biceps. By studying the sEMG signal of the biceps, we can search for the relationship between elbow interaction force and sEMG signals.

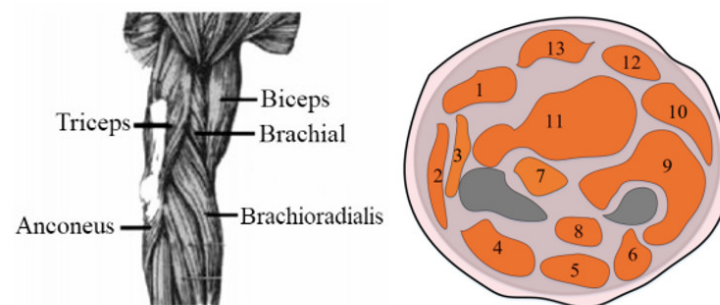


**Figure 2.** Elbow joint muscle contribution during isometric contraction. In order: 1. Extensor Carpi Radialis Longus, 2. Flexor Digitorum, 3. Pronator Teres, 4. Extensor Digitorum Communis, 5. Palmaris Longus, 6. Extensor Carpi Ulnaris, 7. Flexor Pollicis Longus, 8. Extensor Pollicis Longus, 9. Brachioradialis, 10. Flexor Pollicis Longus, 11. Biceps, 12. Flexor Carpi Ulnaris, 13. Flexor Carpi Radialis.

### 2.2. Signal Preprocessing

Under ideal conditions, the sEMG signal is superimposed by the signals of the muscle units involved in the body movement, and they would not crosstalk each other [26]. Signal analysis-based force estimation methods depend on extracting the biological signal components. However, most sEMG signals are composed of many different components, including background noise, resistive noise, and scatter-shot noise. Therefore, the sEMG signal is a time series signal coupled with the nonlinear and non-stationary feature, which has the characteristics of weak strength, a low-frequency range, and large randomness. This dynamically stochastic feature of the sEMG signal affects the reliability and accuracy of the muscle force estimation. It is often difficult for the traditional signal analysis-based force estimation methods to identify the different signal components and extract effective features.

To decompose the nonlinear and non-stationary part, we introduce the moving average filter to separate the raw sEMG sequence for more convenience and effectiveness. After that, the nonlinearity data are normalized by using the sliding window technique.

Suppose the sEMG acquisition system collected the raw sEMG time series which is noted by:  $S_t(l) = \{S_t^1, S_t^2, \dots, S_t^l\}$ .

The nonlinearity series part of the raw sEMG series can be obtained by the sliding average filter, noted by:  $MS_t(l) = \{MS_t^1, MS_t^2, \dots, MS_t^l\}$ ,

$$MS_t^k = \begin{cases} \frac{S_t^1 + S_t^2 + \dots + S_t^l}{k}, & k = 1, 2, \dots, w_1 - 1 \\ \frac{S_t^{k-w_1+1} + S_t^{k-w_1+2} + \dots + S_t^l}{w_1}, & k = w_1, w_1 + 1, \dots, L \end{cases} \quad (1)$$

where  $w_1 (w_1 < L)$  is the sliding window size;  $S_t^l$  denotes the raw sEMG data at time step  $l$ ;  $MS_t^k$  denotes the sEMG nonlinearity data at time step  $k$ .

Muscle contraction is a continuous process, so we adopted a sliding window with an overlapping window to divide the entire sEMG series into multiple discrete time series by sliding window. The process of this algorithm is shown in Figure 3. Considering that the nonlinear sequence has strong characteristics of time series, and historical data hide rich operating experience, we presumed that  $W_x$  is window size, and sEMG time-series signals are divided into several segments by the window. Let,  $x_i = S_t(l), \bar{x}_t = MS_t^l$ ,

$$x_i = (\bar{x}_{t-T_x+1}, \bar{x}_{t-T_x+2}, \dots, \bar{x}_t) \quad (2)$$

$$t = T_x, T_x + \Delta t, T_x + 2\Delta t, \dots$$

where  $\Delta t$  is the slide step,  $t$  is the window size.

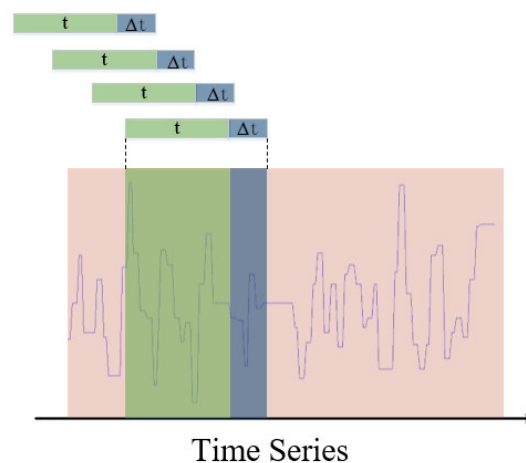


Figure 3. Fix-length slide window algorithm.

### 2.3. Our Proposed Framework

#### 2.3.1. Feature Extraction

The traditional force estimation methods used the statistics of the extracted features from the biological signal [27]. However, all those methods require manual parameter tuning for feature extraction, which leads to poor accuracy and higher sensitivity to the noise. It is difficult to extract the valid features of sEMG using a manual method due to the non-stationary characteristic and the nonlinearity of sEMG. Deep learning methods have been widely used in feature extraction. Studies have proved that the deep neural network is more effective in the feature extracting of one-dimensional time series [28]. CNN is a kind of feed-forward neural network which includes a convolution operation and deep structure. The essential characteristics of this network are local perception and parameter sharing. It can realize the high-dimensional representation of the original data and extract valid spatial features from the original input data. In 2016, He et al. [29] proposed the ResNet based on the cross-layer connection principle of the VGGNet to effectively solve the degradation phenomenon, and the input  $x$  is mapped and added to the output feature. The framework of ResNet is shown in Figure 4. In this section, we used ResNet to extract the different features of electromyography. It is a one-dimensional operation on two-dimensional input data, and it was used to extract the spatial features of the time series from the input. The network consists of the convolution layer, pooling layer, and the residual block, which showed as follows:

#### (1) Convolutional Layer

The convolution layer is mainly used to extract the features of local regions by the convolution operation of sEMG time series segment  $x_i$ . Different convolution kernels extract different time series features, and the convolution operation can be expressed as:

$$x_j = f \left( \sum_i k^{i,j} * x^i + b^j \right) \quad (3)$$

where,  $x^i$  represents the input time series of  $i$ th layer,  $x_j$  represents the feature of  $j$ th layer,  $k^{i,j}$  represents the convolution kernel,  $f(\cdot)$  represents the ReLU activation function.

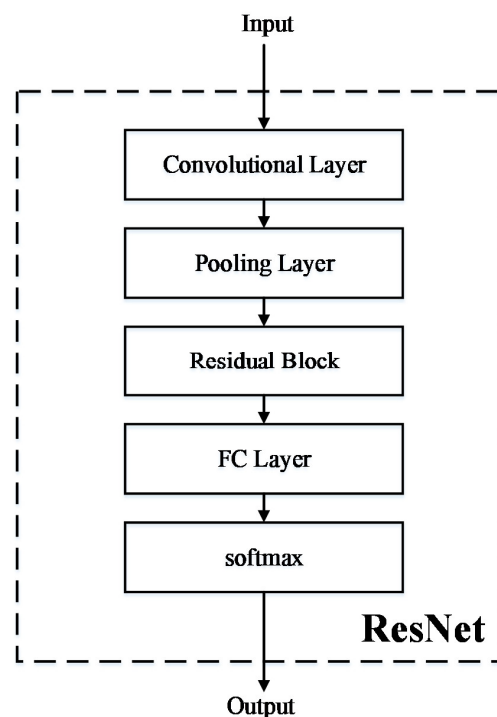


Figure 4. ResNet framework.

(2) Pooling Layer

The pooling layer mainly conducts feature selection by subsampling the output of the convolutional layer, which can reduce the feature size. We adopt the average pool method, and the expressions are as follows:

$$y_{ij} = \frac{1}{c^2} \left( \sum_{i=1}^c \sum_{j=1}^c F_{ij} \right) + b \tag{4}$$

$$y_{ij} = \sum_{i=1, j=1}^c \max(F_{ij}) + b \tag{5}$$

$F$  represents the input of the feature matrix, and  $c$  is the moving step.

(3) Residual Learning

Residual learning is the core of ResNet, whose main feature is the introduction of the concept of “shortcut connection” by establishing residual blocks. The schematic diagram of the residual block is shown in Figure 5.

The output feature  $H(x)$  is expressed as:

$$H(x) = F(x) + x \tag{6}$$

where,  $F(x)$  is a residual error,  $x$  is input.

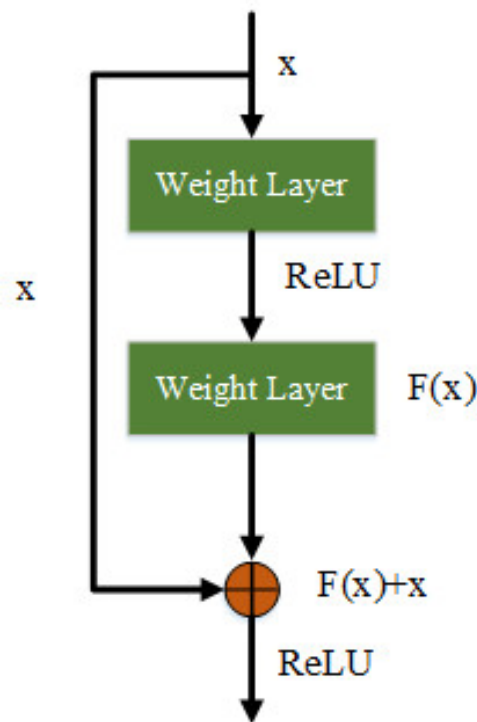


Figure 5. Schematic diagram of residual block.

2.3.2. Force Estimation

A Recurrent Neural Network (RNN) is a computational model designed to deal with the temporal features of the input signal. It is quite similar to a feed–forward neural network, and it can cycle in the network. The network can realize memory through the cycle, allowing it to combine the current input with the past several time steps.

LSTM network is a branch of RNN that can remember the previous information and keep the error at a constant level [30]. It can let the recursive network establish a long distance connection. LSTM is quite suitable for processing time sequence data. It can exploit long–range dependencies in time series data and can furthermore lead to more

efficient force estimation. Figure 6 shows the unit composition of the LSTM block which consists of the input gate, forget gate, and the output gate. The calculation process of LSTM can be summarized as follows: Calculate the useful information for the next moment by forgetting the information in the current cell state and memorizing new information from the new cell. The useless information needs to be discarded, and a hidden state will be output at each time step.

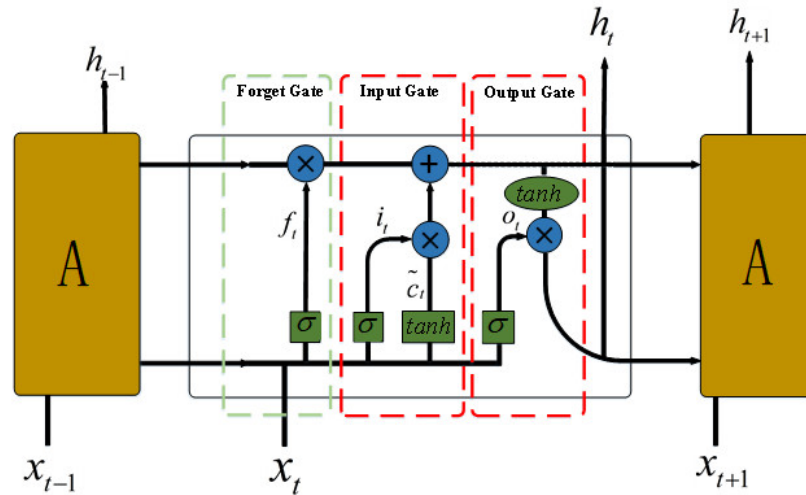


Figure 6. Unit composition of the LSTM block.

Forget Gate: The information to be saved is determined by the current input, the state at the previous moment, and the output of the previous moment.

$$f_t = \sigma(W_f \cdot [h_{t-1}, x_t] + b_f) \tag{7}$$

where  $h_{t-1}$  is hidden state of the previous moment,  $x_t$  is the current input,  $W_f$  is the weight parameter,  $b_f$  is bias, and  $f_t$  is the output of the forget gate.

Input Gate: Memorize the information you need to remember.

$$i_t = \sigma(W_i \cdot [h_{t-1}, x_t] + b_i) \tag{8}$$

$$\tilde{C} = \tanh(W_C \cdot [h_{t-1}, x_t] + b_C) \tag{9}$$

where  $h_{t-1}$  is the hidden state of the previously hidden layer,  $x_t$  is the current input,  $b_i$ ,  $b_C$  is bias term,  $i_t$  is the output of the input gate, and  $\tilde{C}$  is the candidate information of the unit memory at the current moment.

Status updates: Calculates the current cell state at the moment.

$$C_t = f_t * C_{t-1} + i_t * \tilde{C}_t \tag{10}$$

where  $i_t$  is the output of the input gate,  $f_t$  is the output of forget gate,  $C_{t-1}$  is the cellular state of the previous moment,  $\tilde{C}_t$  is the temporary cellular state.

Output Gate: The information to be output is determined based on the latest state, the output of the previous moment, and the current state.

$$o_t = \sigma(W_o [h_{t-1}, x_t] + b_o) \tag{11}$$

$$h_t = o_t * \tanh(C_t) \tag{12}$$

where,  $o_t$  is the output of the output gate,  $h_{t-1}$  is the hidden state of the previously hidden layer,  $x_t$  is current input,  $b_o$  is bias term,  $h_t$  is the hidden state,  $C_t$  is the cellular state of the current moment.

However, there were two common problems with the model using LSTM: the vanishing gradient problem and the inability to encode information back to the front. BiLSTM networks mitigate this problem by combining two normal LSTMs, information can flow both in the forward and backward time direction. The structure of BiLSTM consists of a forward LSTM cell and a backward LSTM cell. Figure 7 shows a schematic of a BiLSTM. Where the  $X_1, X_2, \dots, X_T$  represent the outputs of the previous layer.

sEMG features series contain different temporal information, and not all features contribute equally to the estimate of force. By introducing an attention mechanism, encoding the full input sequences into a fixed-length vector is no longer needed. A neural network with attention mechanism has recently shown success in a wide range of tasks, such as machine translation, time series prediction, and speech recognition [31–33]. In this part, we employed an attention mechanism to improve the learning efficiency and ability to learn important features for regression tasks.

$$P(y_t|y_1, y_2, \dots, y_{t-1}, X) = g(y_{t-1}, s_t, C_t) \tag{13}$$

$$s_t = f(s_{t-1}, y_{t-1}, C_t) \tag{14}$$

$$C_t = \sum_{i=1}^T \alpha_{t,i} h_i \tag{15}$$

$$\alpha_{t,i} = \frac{\exp(e_{t,j})}{\sum_j^T \exp(e_{t,j})} \tag{16}$$

$$e_{t,j} = \text{score}(s_{t-1}, h_i) \tag{17}$$

where,  $y_1, y_2, y_{t-1}, y_t$  is output at time step 1, 2,  $t - 1, t$ , respectively,  $X$  is the input of the current moment,  $C_t$  is the output of the BiLSTM model,  $\alpha_{t,i}$  is the weight of the attention layer, the score is the inner product,  $h_i$  is output of hidden layer,  $s_{t-1}$  is a summary of the previous period which from 0 to  $(t - 1)$  time step.

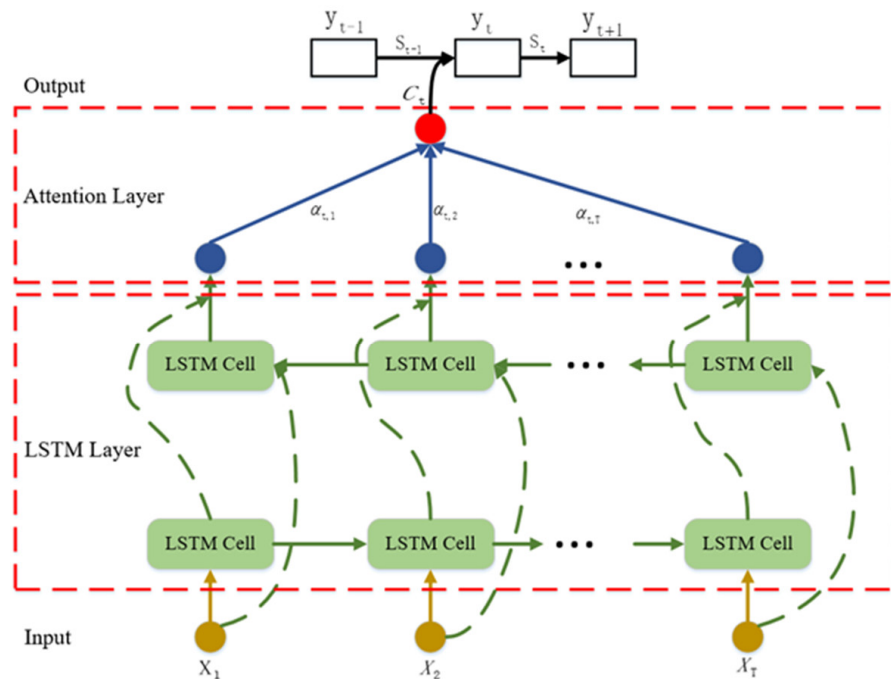


Figure 7. Schematic of BiLSTM Network.

## 2.4. Training Process

### 2.4.1. Optimizer

Although the stochastic gradient descent algorithm (SGD) is effective in most cases, it does not easily jump out of the region of the local optimal solution. To solve this problem, the idea of momentum was introduced into the SGD [34]:

$$g_t = \nabla_{\theta_{t-1}} f(\theta_{t-1}) \quad (18)$$

$$\nabla_{\theta_t} = -\eta * g_t \quad (19)$$

$$m_t = \mu * m_{t-1} + g_t \quad (20)$$

where,  $g_t$  is the gradient of step  $t$ ,  $\eta$  is the learning rate,  $m_t$  is the sum of the current momentum,  $\mu$  is the momentum factor that is used to adjust the importance of the previous step's momentum to the parameter update.

### 2.4.2. Cost Function

Since the ResNet network is a multi-feature classification model, the most commonly used cost function is the cross-entropy cost function:

$$J_1 = -\frac{1}{m} \sum_{n=1}^m [y^{(n)} \log \hat{y}^{(n)} + (1 - y^{(n)}) \log (1 - \hat{y}^{(n)})] \quad (21)$$

where,  $y^{(n)}$  represents the input value,  $\hat{y}^{(n)}$  represents the expected value.

In the BiLSTM model, we chose the mean square error cost function which is suitable for regression problems:

$$J_2 = \frac{1}{N} \sum_{i=1}^N (y_i - y_p)^2 \quad (22)$$

where,  $y_i$  represents the actual value,  $y_p$  represents the estimated value.

### 2.4.3. Learning Rate

Learning rate is a crucial hyper-parameter in the training process of deep learning. Too low a learning rate will cause the loss function to change too slowly. Although you will not miss any local minimum, it will take longer to converge, especially if you are trapped in a highland region [35,36]. Therefore, the fixed learning rate decay method is adopted in our model, which is defined as:

$$\alpha = \frac{1}{(1 + decay\_rate * epoch)} * lr \quad (23)$$

where  $\alpha$  is learning rate,  $decay\_rate$  is attenuation,  $epoch$  is iterations,  $lr$  is initial learning rate which is set as 0.0001.

### 2.4.4. Overfitting

Dropout is adopted into our framework. It uses the idea of model averaging as a great way to prevent one neuron from becoming overly dependent on another [37].

## 2.5. Evaluation

In this paper, we chose the Normalized Root Mean Square Error (NRMSE) and coefficient of determination ( $R^2$ ) as the evaluation indexes of algorithm performance [38]. The definition of The NRMSE is as follows:

$$\text{NRMSE} = \frac{\sqrt{\frac{1}{n} \sum_{i=1}^n (y_i - \tilde{y}_i)^2}}{\tilde{y}_{imax} - \tilde{y}_{imin}} \quad (24)$$

where,  $y_i$  is actual force,  $\tilde{y}_i$  is estimated force,  $\tilde{y}_{i\min}$  is the minimum of the actual force,  $\tilde{y}_{i\max}$  is the mean value of actual force.

The derivation of the coefficient of determination is as follows:

1. Calculate the total sum of squares (TSS):

$$\text{TSS} = \sum (y_i - \bar{y}_i)^2 \quad (25)$$

where, the  $\bar{y}_i$  represents the average value.

2. Calculate the sum of squares for error (SSE):

$$\text{SSE} = \sum (\tilde{y}_i - y_i)^2 \quad (26)$$

where, the  $y_i$  represents the actual value,  $\tilde{y}_i$  represents the predicted value.

3. The coefficient of determination ( $R^2$ ) is used to evaluate the fit of the network:

$$R^2 = 1 - \frac{\text{SSE}}{\text{TSS}} = \frac{\sum (\tilde{y}_i - y_i)^2}{\sum (y_i - \bar{y}_i)^2} \quad (27)$$

### 3. Results

#### 3.1. Subjects and Experimental Setup

We chose five healthy adults with a mean age of  $24 \pm 3$  years who participated in our experiment. All subjects were given adequate information about the purpose and procedure of the study and each subject's informed consent was obtained before participation. This experiment was approved by the Medical Ethics Committee of Hefei Institutes of Physical Sciences, Chinese Academy of Sciences, Hefei, China. The physical parameters of each subject are shown in the Table 1.

**Table 1.** The physical parameters of each subject.

Subject	Gender	Age	Mass (kg)	Height (cm)
A1	Male	27	77	176
A2	Male	26	70	180
A3	Male	22	80	170
A4	Female	22	52	165
A5	Female	23	48	161

The interaction force is estimated while the elbow joint is performing isometric contraction. As shown in Figure 8A, considering the physiological characteristics of human hand movement and the corresponding major muscles during contraction, the most common flexion and extension movements of hand movement were selected in this experiment. The three main muscles involved in the exercise were chosen: biceps brachii, brachialis, brachioradialis. The subjects were asked to sit in a chair and the right elbow joint was fixed at a different angle ( $30^\circ, 60^\circ, 90^\circ, 120^\circ$ ) through the joint retainer and positioned on the test desk for isometric contraction. Three sEMG sensors were placed at each end of the belly of the muscle (an area without muscle activity was selected as a reference electrode to exclude voltages not generated by the human body autonomously). The sEMG sensor is a double conduction muscle electrical module that consists of analog circuit acquisition and digital signal filter processing. The sampling frequency was set to 1000 Hz. The six-axis force sensor independently designed by the Institute of Intelligent Machines (IIM), Chinese Academy of Sciences (CAS) was utilized for our experiments. The prototype and internal structure of a six-axis force sensor are shown in Figure 8B,C. We only selected the Z axis to measure the interaction force at the end of the upper limb. The parameters of force sensor and sEMG sensor are shown in Table 2. We can compare the estimated force and actual force in real-time through the monitor. The process of our experiment is

described in detail as follows: The five subjects performed three repeated rounds of the experiment in sequence, and each round was completed in three stages. 1. Complete 100% MVC (Maximum Voluntary Contraction) isometric contraction task within 1 s; 2. Complete 100% MVC isometric contraction task within 2 s; 3. Complete the 100% MVC isometric contraction task within 3 s. The experiment procedures for each subject is shown in Table 3. Each subject was required to get sufficient rest after each contraction task before performing the next one. However, due to the different physical conditions of the subjects, the length of rest required was different. There is no exact way to get the amount of rest one needs. In order to ensure the consistency of the experiment, in this experiment we stipulate a 10-s rest after the completion of each contraction task, which is long enough.

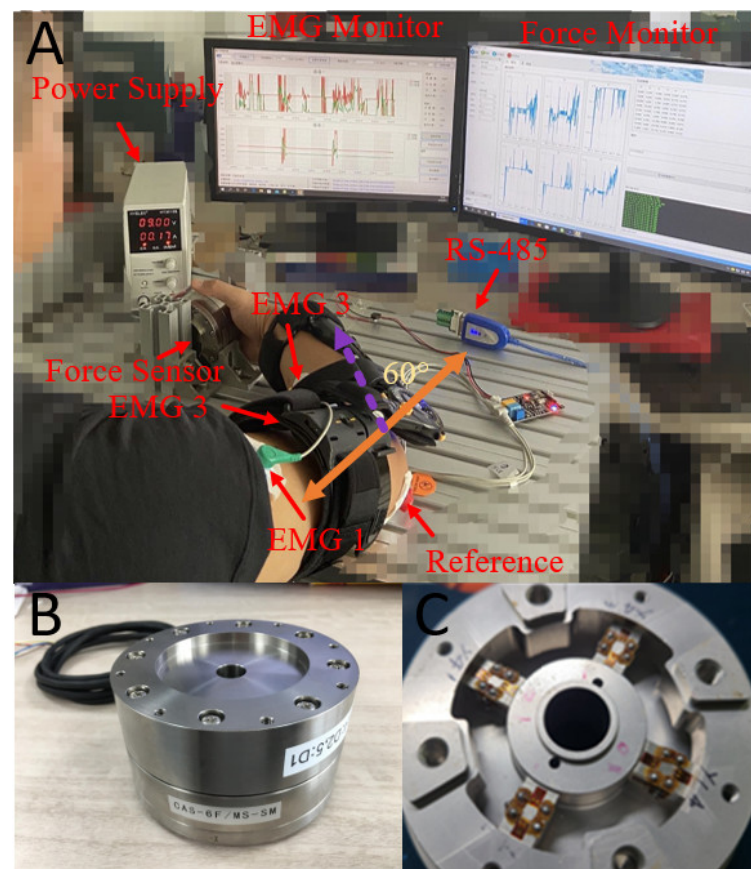


**Figure 8.** (A) System layout in the experiment. The elbow flexion was performed under isometric contraction, and the interaction force was measured by six-axis force sensor. sEMG sensor electrodes were placed on the muscle belly of the biceps brachii, brachialis and brachioradialis to collect the sEMG signal. (B) The prototype of our six-axis force sensor. (C) The internal structure of our six-axis force sensor.

**Table 2.** Parameters of force sensor and sEMG sensor.

Parameters	Force Sensor	sEMG Sensor
Model	CAS-6F/MS-SM	EDK0056
Power supply voltage	DC(9V)	DC(5V)
Temperature range	−30 °C~70 °C	−20 °C~60 °C
Output Signal	Analog Signal	Analog Signal
Maximum of output	1000 N	4.5 V
Communication	RS-485	Bluetooth 4.0

**Table 3.** Experiment procedures for each subject.

Angle	Time			
	1 s	2 s	3 s	
30°	100% (MVC)	100% (MVC)	100% (MVC)	100% (MVC)
60°	100% (MVC)	100% (MVC)	100% (MVC)	100% (MVC)
90°	100% (MVC)	100% (MVC)	100% (MVC)	100% (MVC)
120°	100% (MVC)	100% (MVC)	100% (MVC)	100% (MVC)

### 3.2. Verification

#### 3.2.1. Signal Decoupling

We used the moving average filter method to separate the raw sEMG time series into nonlinearity time series and non-stationary time series. The chosen sliding window size  $w_1$  ( $w_1 < L$ ) is 8. Figure 9 shows the filter effect on the raw sEMG time series of the biceps. Considering the limited space of the picture display, part of the data under 1 s, 2 s, and 3 s contraction tasks were captured and connected to facilitate the comparison of the effectiveness of the algorithm.

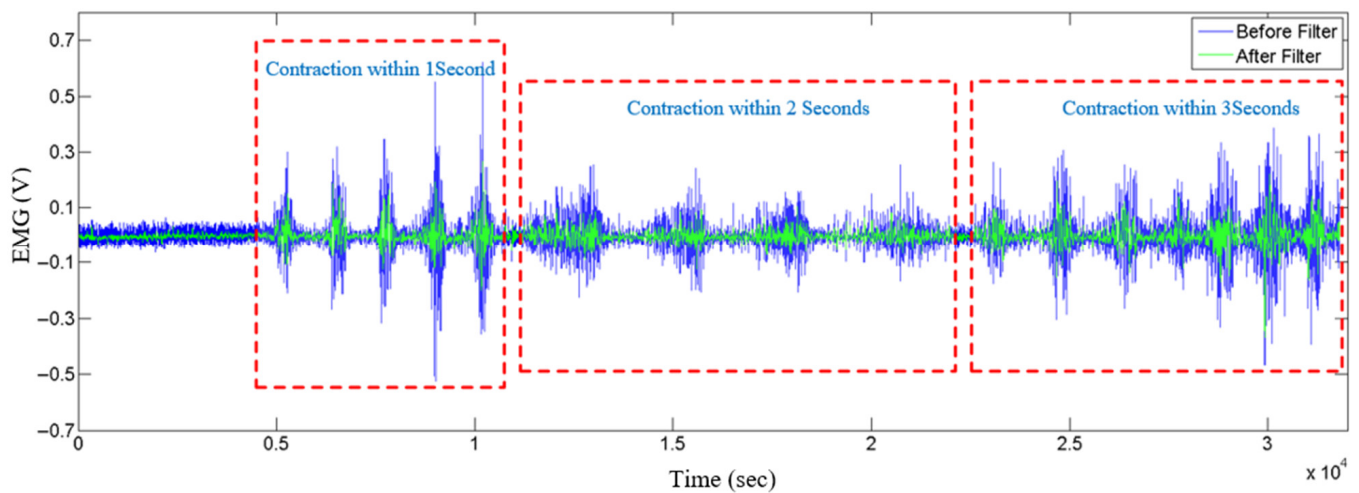


**Figure 9.** Filter effect on the sEMG raw data.

#### 3.2.2. Force Estimation

In order to optimize the network, accelerate the training speed, and improve the accuracy of prediction results, in this experiment, we used the set-aside method to divide the training set and the test set, and increase the proportion of the training set. As a result, we divided the datasets into a training part and a test part with a ratio of 8:2 to verify the performance of the model. To get the best performance of the model, the parameters of the models were fully tuned. Table 4 lists the hyper-parameters of our model, which show the layers, activation function, optimizer, dropout, initial learning rate, batch size, and epoch.

**Table 4.** Hyper-parameters of our model for the dataset.

Hyper-Parameters	ResNet	BiLSTM
Layers	101	128–128
Activation Function	ReLU	ReLU
Optimizer	Momentum	Momentum
Dropout	0.5	0.5
Initial Lr	0.0001	0.0001
Batch Size	128	128
Epoch	1000	1000

We compared the experimental results under three contraction times (1, 2, and 3 s), as shown in Figure 10. The subfigure (a–c) shows the raw sEMG signal. The subfigure (d–f) shows the EMG signal processed by the decoupling algorithm. The subfigure (g–i) shows the comparison between the actual measured interaction force and the predicted force. The subfigure (j–l) shows the mean absolute error of the actual measured interaction force and the predicted force.

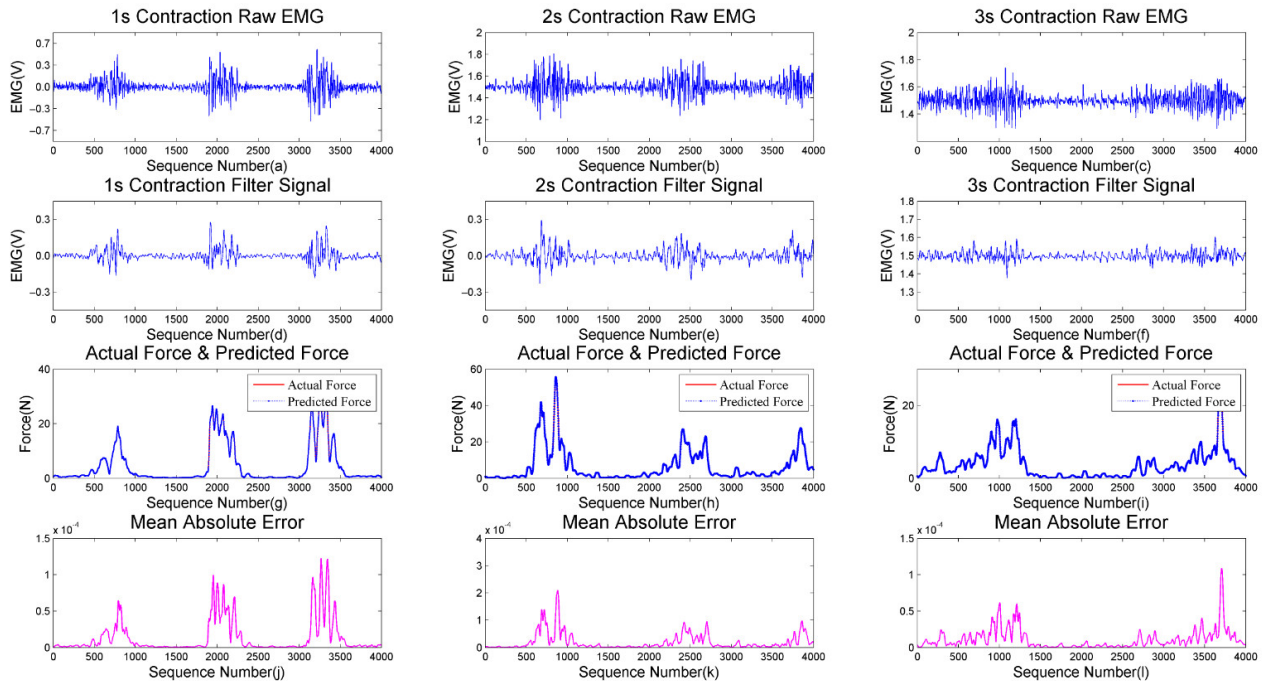


**Figure 10.** Above are experimental results under three contraction conditions (1, 2, 3 s); (a–c) are the raw signal of sEMG; (d–f) are filtered signals after the decoupling algorithm; (g–i) are the comparisons of actual force and predicted force; (j–l) are the mean absolute error of the actual force and the predicted force.

In order to comprehensively evaluate the effectiveness of the algorithm, NRMSE and coefficient of determination are taken into account to evaluate the performance of the model [39,40], which are shown as below. The different window size, joint angle, and other state of the art methods were compared, and the comparison results are shown in Figures 11 and 12.

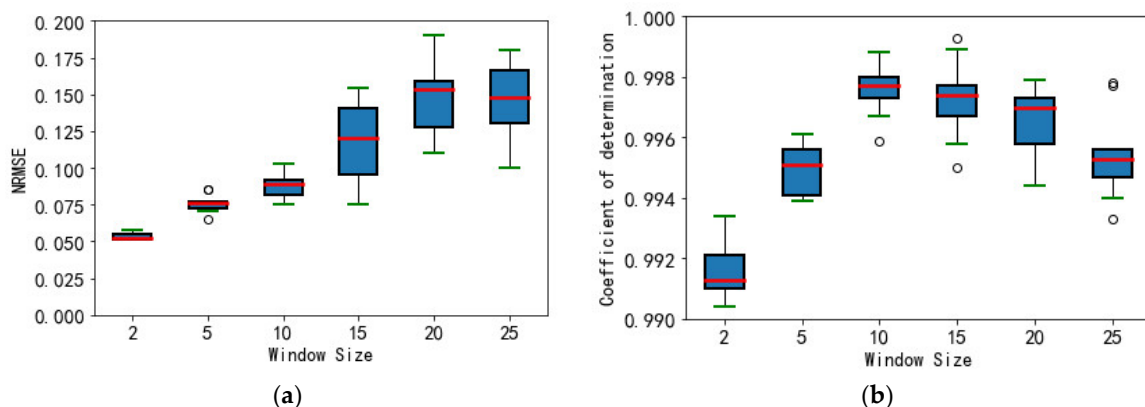


**Figure 11.** Box diagram of evaluation of window size in the algorithm: (a) NRMSE; (b) Coefficient of Determination.

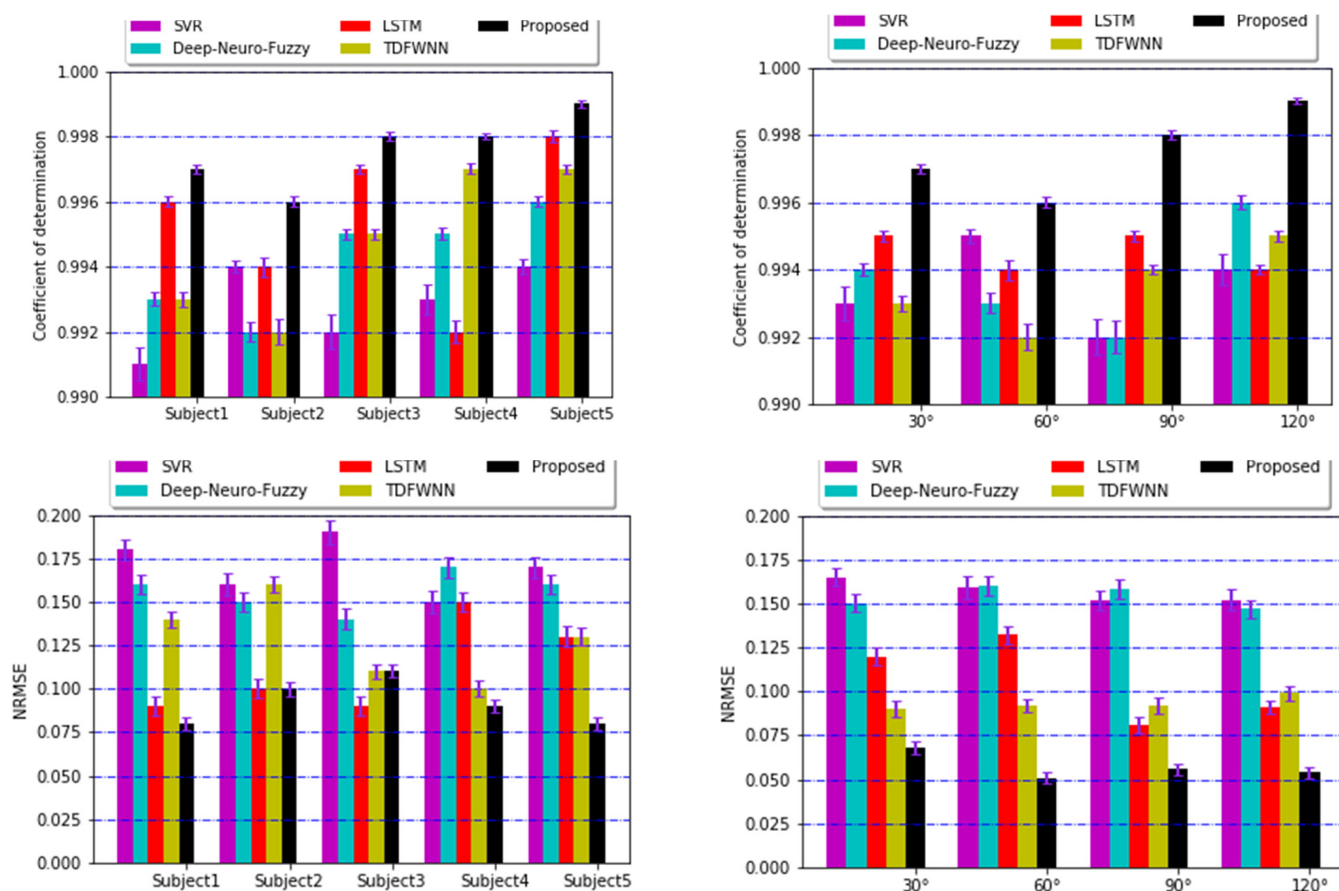


**Figure 12.** Accuracy comparison of different algorithms (NRMSE and Coefficient of determination).

Based on the results shown in Figures 11 and 12, it can be concluded that: (1) For a given subject, our algorithm can obtain accurate estimation results for three different contraction ways. (2) It is very important to select the appropriate window size; too small a window results in the information between adjacent data not being fully mined, whereas too large a window will reduce the effect of estimation.

Based on the results shown in Figure 12, it can be concluded that: (1) In different subjects, our algorithm achieved the best performance in coefficient of determination and NRMSE. LSTM is inferior to our algorithm and SVR is the worst. (2) Under the angle of 30°, each algorithm has achieved good results. The reason is that the muscle would contract to the maximum at the fastest rate. The sEMG signal is less affected by non-stationary factors which are good for estimation performance.

#### 4. Discussion

From the performance comparison of different aspects several main findings were obtained by comparing the performance of the SVR/LSTM/Deep-Neuro-Fuzzy/TDFWNN/ResNet-BiLSTM based on attention.

Firstly, the deep learning network (ResNet-BiLSTM) achieves the best performance. Our framework can capture the local dependence between the temporal dimension and spatial location. It is more suitable for extracting and estimating time-series data. Secondly, the attention mechanism enabled ResNet-BiLSTM to obtain better generalization ability, which could automatically learn feature weights and extract important features of the sEMG signal.

In addition, since the duration of muscle contraction is longer than the size of the sliding window, the results proved that our model can still achieve good performance.

This may be because the long-term shrinkage activity can be regarded as a composition of several short-term shrinkage patterns. The model can find and extract motion features even if the window size cannot contain a complete shrinkage pattern.

## 5. Conclusions

In this work, we present an elbow interaction force estimation algorithm to establish the relationships between the sEMG signal and the elbow interaction forces. Considering the advantages of deep learning technology in nonlinear regression, a ResNet–BiLSTM algorithm is proposed. In the experiment, we used the sEMG signals processed by decoupling and window algorithm as the input of the ResNet–BiLSTM network. The experiment used four subjects to complete a task three times at four angles. The results show that the ResNet–BiLSTM method can accurately estimate the elbow interaction force. The method improves the force required for the motion control of the wearable assisted robot. At the same time, it provides effective input information for human motion intention recognition.

## 6. Future Works

In the future, further research can be conducted on the following aspects:

- (1) To improve the accuracy and robustness of muscle force estimation, it is necessary to develop a multi-signal fusion method.
- (2) We will apply the estimation results of elbow interaction force to the identification of human upper limb motion intention to provide accurate information for rehabilitation assistance equipment.

**Author Contributions:** Data curation, W.L.; Formal analysis, H.C.; Funding acquisition, L.G.; Investigation, H.C.; Methodology, W.L.; Supervision, Z.L.; Validation, L.G. and Z.L.; Visualization, W.L.; Writing—original draft, W.L.; Writing—review&editing, H.C. and Z.L. All authors have read and agreed to the published version of the manuscript.

**Funding:** This research was funded by the Strategic Priority Research Program of the Chinese Academy of Sciences, Grant No. XDA22040303. Key Research and Development Project of Anhui Province, Grant No. 2022a05020035. Major Science and Technology Project of Anhui Province, Grant No. 202103a05020022. Key Research Projects Supported by the National Natural Science Foundation of China, Grant No. 92067205. Natural Science Foundation of Anhui Province, Grant No. 1808085QF514. Key scientific research projects of Anhui Province higher education, Grant No. KJ2020A0630.

**Institutional Review Board Statement:** Ethical review and approval were approved by the Institutional Review Committee of Hefei Institute of Physical Science, Chinese Academy of Sciences. The approval number is no. SWYX-Y-2021-75. All subjects are composed of students and staff of the research group; no patients are involved. Moreover, there is no harm to the body in our experiment.

**Informed Consent Statement:** Informed consent was obtained from all subjects involved in the study.

**Data Availability Statement:** The data used to support the findings of this study are included within the article.

**Acknowledgments:** This work was partly carried out at the Robotic Sensors and Human-Computer Interaction Laboratory, Hefei Institute of Intelligent Machinery, Chinese Academy of Sciences.

**Conflicts of Interest:** The authors declare no conflict of interest.

## References

1. Ding, H.; Yang, X.; Zheng, N. Tri-Co robot: A Chinese robotic research initiative for enhanced robot interaction capabilities. *Natl. Sci. Rev.* **2017**, *485*, nwx148. [[CrossRef](#)]
2. Sirintuna, D.; Ozdamar, I.; Aydin, Y. Detecting Human Motion Intention during pHRI Using Artificial Neural Networks Trained by EMG Signals. In Proceedings of the 29th IEEE International Conference on Robot and Human Interactive Communication (RO-MAN), Naples, Italy, 31 August–4 September 2020.
3. Pan, C.T.; Chang, C.C.; Yang, Y.S. Development of MMG sensors using PVDF piezoelectric electrospinning for lower limb rehabilitation exoskeleton. *Sens. Actuators A Phys.* **2019**, *301*, 111708. [[CrossRef](#)]

4. Hu, X.; Tong, K.; Li, L. The mechanomyography of persons after stroke during isometric voluntary contractions. *J. Electromyogr. Kinesiol.* **2007**, *17*, 473–483. [[CrossRef](#)] [[PubMed](#)]
5. Wang, M.; El Fiqi, H.; Hu, J.; Abbasss, H.A. Convolutional neural networks using dynamic functional connectivity for EEG-based person identification in diverse human states. *IEEE Trans. Inf. Forensics Secur.* **2019**, *14*, 3359–3372. [[CrossRef](#)]
6. Mithbavkar, S.; Shah, M. Recognition of Emotion in Indian Classical Dance Using EMG Signal. *Int. J. Adv. Sci. Eng. Inf. Technol.* **2021**, *11*, 1336. [[CrossRef](#)]
7. Yao, S.; Zhang, Y.; Li, Z.; Song, R. Adaptive Admittance Control for an Ankle Exoskeleton Using an EMG-Driven Musculoskeletal Model. *Front. Neurobot.* **2018**, *12*, 16. [[CrossRef](#)] [[PubMed](#)]
8. Farina, D.; Jiang, N.; Rehbaum, H. The extraction of neural information from the surface EMG for the control of upperlimb prostheses: Emerging avenues and challenges. *IEEE Trans. Neural Syst. Rehabil. Eng.* **2014**, *22*, 797–809. [[CrossRef](#)] [[PubMed](#)]
9. Pang, M.; Guo, S.; Huang, Q.; Ishihara, H.; Hirata, H. Electromyography-based quantitative representation method for upperlimb elbow joint angle in sagittal plane. *J. Med. Biol. Eng.* **2015**, *35*, 165–177. [[CrossRef](#)] [[PubMed](#)]
10. Romero, F.; Alonso, F.J. A comparison among different Hill-type contraction dynamics formulations for muscle force estimation. *Mech. Sci.* **2016**, *7*, 19–29. [[CrossRef](#)]
11. Buchanan, T.S.; Lloyd, D.G.; Manal, K.; Besier, T.F. Estimation of muscle forces and joint moments using a forward-inverse dynamics model. *Med. Sci. Sports Exerc.* **2005**, *37*, 1911–1916. [[CrossRef](#)]
12. Hayashibe, M.; Guiraud, D.; Poignet, P. EMG-to-force estimation with full-scale physiology based muscle model. *Intell. Robot. Syst.* **2009**, *6*, 1621–1626.
13. Na, Y.; Choi, C.; Lee, H.-D.; Kim, J. A Study on Estimation of Joint Force Through Isometric Index Finger Abduction with the Help of SEMG Peaks for Biomedical Applications. *IEEE Trans. Cybern.* **2016**, *46*, 2–8. [[CrossRef](#)] [[PubMed](#)]
14. Na, Y.; Kim, S.J.; Kim, J. Force estimation in fatigue condition using a muscle-twitch model during isometric finger contraction. *Med. Eng. Phys.* **2017**, *50*, 103–108. [[CrossRef](#)]
15. Youn, W.; Kim, J. Estimation of elbow flexion force during isometric muscle contraction from mechanomyography and electromyography. *Med. Biol. Eng. Comput.* **2010**, *48*, 1159. [[CrossRef](#)]
16. Wang, D.Q.; Wu, H.F.; Xie, C.L.; Gao, L.F. Suppression of Motion Artifacts in Multichannel Mechanomyography Using Multivariate Empirical Mode Decomposition. *IEEE Sens. J.* **2019**, *19*, 5732–5739. [[CrossRef](#)]
17. Allouch, S.; Harrach, M.A.; Boudaoud, S.; Laforet, J.; Younes, R. Muscle force estimation using data fusion from high-density SEMG grid. In Proceedings of the 2nd IEEE International Conference on Advances in Biomedical Engineering (ICABME), Tripoli, Lebanon, 11–13 September 2013.
18. Xia, P.; Hu, J.; Peng, Y. EMG-Based Estimation of Limb Movement Using Deep Learning with Recurrent Convolutional Neural Networks. *Artif. Organs* **2018**, *42*, E67. [[CrossRef](#)]
19. Duan, F.; Dai, L.; Chang, W.; Chen, Z.; Zhu, C.; Li, W. sEMG-Based Identification of Hand Motion Commands using Wavelet Neural Network Combined with Discrete Wavelet Transform. *IEEE Trans. Ind. Electron.* **2016**, *63*, 1923–1934. [[CrossRef](#)]
20. Wu, H.; Huang, Q.; Wang, D. A CNN-SVM combined model for pattern recognition of knee motion using mechanomyography signals. *J. Electromyogr. Kinesiol.* **2018**, *42*, 136–142. [[CrossRef](#)]
21. Xie, C.; Wang, D.; Wu, H. A long short-term memory neural network model for knee joint acceleration estimation using mechanomyography signals. *Int. J. Adv. Robot. Syst.* **2020**, *17*, 172988142096870. [[CrossRef](#)]
22. Luo, J.; Liu, C.; Yang, C. Estimation of EMG-Based Force Using a Neural-Network-Based Approach. *IEEE Access* **2019**, *7*, 64856–64865. [[CrossRef](#)]
23. Aviles, A.I.; Alsaleh, S.M.; Montseny, E. A Deep-Neuro-Fuzzy approach for estimating the interaction forces in Robotic surgery. In Proceedings of the 2016 IEEE International Conference on Fuzzy Systems (FUZZ-IEEE), Vancouver, QC, Canada, 24–29 July 2016.
24. Lu, W.; Gao, L.; Zhang, Q. A Hybrid Deep Learning Framework for Estimation of Elbow Flexion Force via Electromyography. *J. Phys. Conf. Ser.* **2021**, *1883*, 012164. [[CrossRef](#)]
25. Zonnino, A.; Sergi, F. Model-based estimation of individual muscle force based on measurements of muscle activity in forearm muscles during isometric tasks. *IEEE Trans. Bio Med. Eng.* **2019**, *67*, 134–145. [[CrossRef](#)] [[PubMed](#)]
26. Plewa, K.; Samadani, A.; Orlandi, S. A novel approach to automatically quantify the level of coincident activity between EMG and MMG signals. *J. Electromyogr. Kinesiol.* **2018**, *41*, 34–40. [[CrossRef](#)] [[PubMed](#)]
27. Ibitoye, M.O.; Hamzaid, N.A.; Abdulwahab, A.K. Prospects of Mechanomyography (MMG) in Muscle Function Assessment during FES Evoked Contraction: A Review. In Proceedings of the 15th International Conference on Biomedical Engineering, Singapore, 4–7 December 2013; Springer: Cham, Switzerland, 2014; Volume 43, pp. 524–526.
28. Lin, H.; Zhao, J.; Liang, S. Prediction model for stock price trend based on convolution neural network. *J. Intell. Fuzzy Syst.* **2020**, *39*, 4999–5008. [[CrossRef](#)]
29. He, K.; Zhang, X.; Ren, S.; Sun, J. Deep residual learning for image recognition. In Proceedings of the IEEE Conference on Computer Vision and Pattern Recognition, Las Vegas, NV, USA, 27–30 June 2016; Volume 6, pp. 770–778.
30. Huan, J.; Li, H.; Li, M. Prediction of dissolved oxygen in aquaculture based on gradient boosting decision tree and long short-term memory network: A study of Chang Zhou fishery demonstration base, China. *Comput. Electron. Agric.* **2020**, *175*, 105530. [[CrossRef](#)]
31. Hermann, K.M.; Kocisky, T.; Grefenstette, E.; Espeholt, L.; Kay, W.; Suleyman, M.; Blunsom, P. Teaching machines to read and comprehend. In *Advances in Neural Information Processing Systems*; MIT Press: Cambridge, MA, USA, 2015; pp. 1684–1692.

32. Yan, X.; Mou, L.L.; Li, G.; Chen, Y.C.; Peng, H.; Jin, Z. Classifying relations via long short term memory networks along shortest dependency path. *arXiv*, 2015; arXiv:1508.03720.
33. Siami-Namini, S.; Tavakoli, N.; Namin, A.S. The Performance of LSTM and BiLSTM in Forecasting Time Series. In Proceedings of the 2019 IEEE International Conference on Big Data (Big Data), Los Angeles, CA, USA, 9–12 December 2019.
34. Zarba, S.; Gonczarek, A.; Tomczak, J.M.; Witek, J. Accelerated learning for Restricted Boltzmann Machine with momentum term. In *Progress in Systems Engineering*; Springer: Cham, Switzerland, 2015.
35. Smith, L.N. Cyclical Learning Rates for Training Neural Networks. In Proceedings of the 2017 IEEE Winter Conference on Applications of Computer Vision (WACV), Santa Rosa, CA, USA, 24–31 March 2017; pp. 464–472.
36. Vidal-Beltrán, S.; Bonilla, J.L.L.; Piñón, F.M.; Yalja-Montiel, J. Gradient Descent Optimization Algorithms for Decoding SCMA Signals. *Int. J. Comput. Intell. Appl.* **2020**, *3*, 2150002. [[CrossRef](#)]
37. Hinton, G.E.; Srivastava, N.; Krizhevsky, A. Improving neural networks by preventing co-adaptation of feature detectors. *arXiv* **2012**, arXiv:1207.0580.
38. Cameron, A.C.; Windmeijer, F.A.G. An R-squared measure of goodness of fit for some common nonlinear regression models. *J. Econ.* **1997**, *77*, 329–342. [[CrossRef](#)]
39. Lu, L.; Wu, Q.; Xi, C. Development of a sEMG-based torque estimation control strategy for a soft elbow exoskeleton. *Robot. Auton. Syst.* **2019**, *111*, 88–98. [[CrossRef](#)]
40. Nurhanim, K.; Elamvazuthi, I.; Izhar, L.I. Development of a model for sEMG based joint-torque estimation using Swarm techniques. In Proceedings of the IEEE International Symposium on Robotics&Manufacturing Automation, Ipoh, Malaysia, 25–27 September 2016.